

# Deep Dual-resolution Networks for Real-time and Accurate Semantic Segmentation of Road Scenes

Yuanduo Hong, Huihui Pan, Weichao Sun, *Senior Member, IEEE*, Yisong Jia

**Abstract**—Semantic segmentation is a critical technology for autonomous vehicles to understand surrounding scenes. For practical autonomous vehicles, it is undesirable to spend a considerable amount of inference time to achieve high-accuracy segmentation results. Using light-weight architectures (encoder-decoder or two-pathway) or reasoning on low-resolution images, recent methods realize very fast scene parsing which even run at more than 100 FPS on single 1080Ti GPU. However, there are still evident gaps in performance between these real-time methods and models based on dilation backbones. To tackle this problem, we propose novel deep dual-resolution networks (DDRNs) for real-time semantic segmentation of road scenes. Besides, we design a new contextual information extractor named Deep Aggregation Pyramid Pooling Module (DAPPM) to enlarge effective receptive fields and fuse multi-scale context. Our method achieves new state-of-the-art trade-off between accuracy and speed on both Cityscapes and CamVid dataset. Specially, on single 2080Ti GPU, DDRNet-23-slim yields 77.4% mIoU at 109 FPS on Cityscapes test set and 74.4% mIoU at 230 FPS on CamVid test set. Without utilizing attention mechanism, pre-training on larger semantic segmentation dataset or inference acceleration, DDRNet-39 attains 80.4% test mIoU at 23 FPS on Cityscapes. With widely used test augmentation, our method is still superior to most state-of-the-art models, requiring much less computation. Codes and trained models will be made publicly available.

**Index Terms**—Semantic segmentation, real-time, deep convolutional neural networks, autonomous driving

## I. INTRODUCTION

SEMANTIC segmentation is a basic task in which each pixel of input images should be assigned to the corresponding label [1]–[3]. It plays a vital role in many practical applications such as medical image segmentation, navigation of autonomous vehicles and robots [4], [5]. With the rise of deep learning technologies, convolutional neural networks are applied to image segmentation and greatly outperform traditional methods. A series of novel networks have been devised to promote effectiveness since fully convolutional network (FCN) [6] was proposed to handle semantic segmentation problems. Since semantic segmentation is a kind of dense prediction task, neural networks need to output high-resolution feature maps of large receptive fields to produce good results, which is computationally dependent. Such problem is especially serious for scene parsing of autonomous driving because it requires enforcement on very large images to cover a wide field of view. DeepLab [7] eliminates some of downsampling in ResNet to maintain high resolution and utilizes convolutions

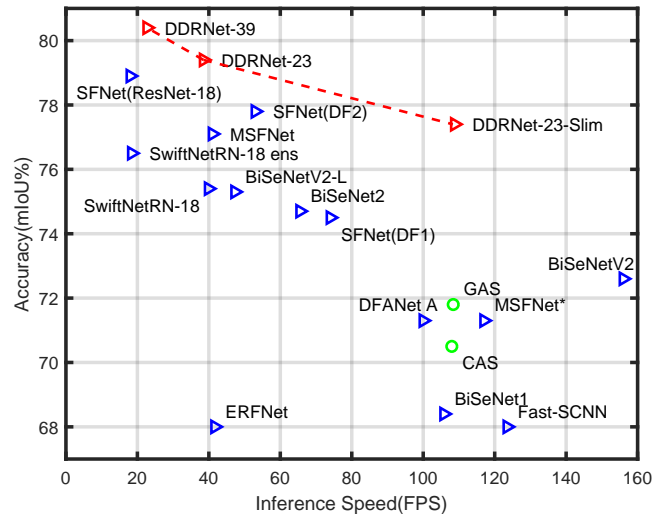


Fig. 1. A comparison of speed-accuracy trade-off on Cityscapes test set. The red triangles indicate our methods while blue triangles represent other methods. Green circles represent architecture search methods.

with large dilations [8] to enlarge receptive fields. Since then ImageNet pre-trained backbones with dilated convolutions have become the standard layout widely used in various methods, including DeepLabV2 [9], DeepLabV3 [10], PSPNet [11] and DenseASPP [12]. However, these methods are very time-consuming during inference which can not be deployed on practical self-driving vehicles. In fact, they even can not process single image in one second because of utilizing multi-scale test to improve accuracy.

Without modifying general ImageNet classification architectures, authors of HRNet [13] directly realize deep high-resolution representation and implement parallel high-to-low resolution subnetworks to enlarge receptive fields. HRNet outperforms previous exemplars including DeepLabV3 and PSPNet on Cityscapes dataset using less computation [14]. But due to its deep multiple branches and multiple repeated fusion of multi-scale feature [13], HRNet seems not to be an ideal choice for real-time semantic segmentation.

With ever-increasing demand of deployment on mobile devices, real-time segmentation algorithms [15]–[19] draw more and more attention. Most of them utilize the light-weight encoder-decoder architectures. DFANet [20] employs deeply multi-scale feature aggregation and achieves 71.3% test mIoU with 100 FPS using lightweight depthwise separable convolutions. Different from encoder-decoder paradigm, authors in [21] propose a novel bilateral network consisted

The authors are with Research Institute of Intelligent Control and Systems, Harbin Institute of Technology, Harbin 150001, China (e-mail: huihuihan@hit.edu.cn)

of a spatial path and a context path. Specially, the spatial path utilizes three relatively wide  $3 \times 3$  convolutional layers to extract spatial details and the context path is a compact pre-trained backbone to learn contextual information. Such bilateral methods including [22] achieve higher accuracy than encoder-decoder structures within real-time inference time.

When it comes to semantic segmentation of road scenes for autonomous driving which is a safety-critical application, we require high-quality semantic segmentation as much as possible and low computation load for deployment. Recently, some competitive methods aiming at semantic segmentation of road scenes were proposed. SwiftNet [23] defends the advantage of pre-training encoder on ImageNet and leverages light-weight lateral connections to upsample. Authors in [24] propose a strategy of multiply spatial fusion and class boundary supervision. FANet [25] achieves a trade-off between speed and accuracy with fast attention module and extra downsampling throughout the network. BiSeNetV2 [26] achieving 72.6% test mIOU at 156 FPS on Cityscapes hits a new peak for bilateral methods in real-time applications. But these works do not show the potential towards more high-quality results, some of these methods may not be easily extended due to deliberately devised architectures and tuned hyper-parameters.

In this paper, inspired by HRNet, we propose a deep dual-resolution network with deep high-resolution representation ability for real-time semantic segmentation of high-resolution images, specially for road-driving images. Our DDRNet starts with one trunk and then is split into two parallel deep branches with different resolution. One deep branch generates relatively high-resolution feature maps and the other extracts rich contextual information by multiple downsampling operations. Multiple bilateral connections are bridged between two branches for efficient information fusion. Besides, we propose a novel module named DAPPM which greatly increases the receptive fields and extracts context information more sufficiently than normal PPM. Before training on semantic segmentation dataset, the dual-resolution network is first trained on ImageNet following common paradigms.

According to extensive experimental results on two popular benchmarks, DDRNet attains an excellent balance between segmentation accuracy and inference speed, and takes up less GPU memory than HRNet during training. Our method achieves new state-of-the-art mIoU on both Cityscapes and CamVid compared to other real-time algorithms without attention mechanism and any extra bells or whistles. With standard test augmentation technology, DDRNet is comparable to state-of-the-art models but requires much less computing resources.

The main contributions are summarized as follows:

- A novel bilateral network with deeply dual resolution is proposed for real-time semantic segmentation. Our network attains new state-of-the-art performance considering inference speed without any extra bells or whistles.
- A novel module is designed to harvest rich context information by combining feature aggregation with pyramid pooling. When integrating it with low-resolution feature maps, it leads to little increase in inference time.

- By simply increasing the width and depth of network, DDRNet achieves a top trade-off between mIoU and FPS among existing methods, from 77.4% mIoU at 109 FPS to 80.4% mIoU at 23 FPS on Cityscapes test set.

## II. RELATED WORK

In recent years, advanced methods on the strength of dilated backbones have boosted the performance of semantic segmentation under many challenging scenes. Contextual information representation is proved to be a key component for scene parsing tasks. However, with more and more attention drawn to real-world applications, many works explore the potential of more light-weight architectures such as encoder-decoder methods and two-pathway methods. Fig. 2 shows overall architectures of popular methods and our methods.

### A. High-performance Semantic Segmentation

Capacity of high-resolution representation is very important for acquiring state-of-the-art results because semantic segmentation is a kind of dense prediction tasks. But receptive fields of neural networks will be too small to learning high-level semantic information if only getting rid of pooling layers of ImageNet classification backbones. It is an acceptable strategy to utilize dilated convolutions to set up long-range connection between pixels while removing the last two downsampling layers [7]. However, it also brings new challenges to real-time inference due to the exponential growth of high-resolution feature-map dimension and insufficient optimization of dilated convolutions. There is a fact that most state-of-the-art models are built on dilation backbones and thus have very low practical value on self-driving scene parsing.

Some works try to explore the substitute of the standard dilation backbone. Authors of DeepLabv3plus [27] propose a simple decoder and fuse upsampled feature maps with low-level feature maps. Such improvement alleviates the requirement of high-resolution representation generated by dilated convolutions. DeepLabv3plus can achieve competitive results though the output stride of encoder is set to 16. HRNet highlights deep high-resolution representations and embodies clear advantages over dilation backbones on semantic segmentation. We argue that higher computational efficiency and inference speed of HRNet owe to its much thinner high-resolution information flows. Taking HRNetV2-W48 [14] for example, dimensions of 1/4-resolution features and 1/8-resolution features are 48 and 96 which are much smaller than the dimensions of pre-trained ResNets [28] with dilation convolutions. Though high-resolution branches of HRNet are much thinner, they can be greatly enhanced by parallel low-resolution branches and repeated multi-scale fusion.

Our work starts from the core concept of HRNet and moves forward more compact architectures, maintaining high-resolution representations and extracting high-level contextual information through two concise trunks. Experimental results demonstrate the great potential of DDRNets.

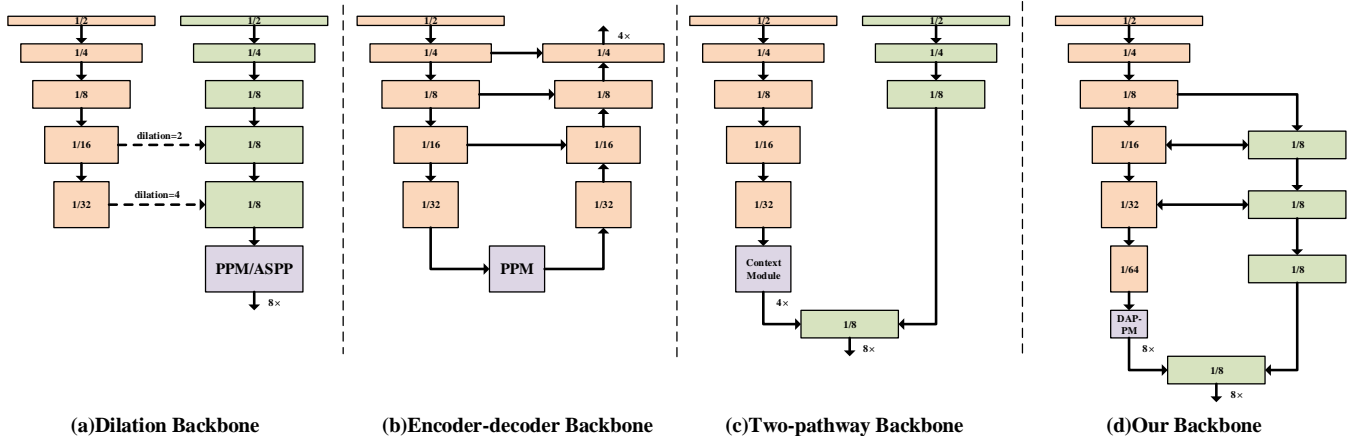


Fig. 2. A comparison about dilation backbone, encoder-decoder backbone, two-pathway backbone and our deep dual-resolution backbone.

### B. Real-time Semantic Segmentation

Almost all the real-time semantic segmentation methods adopt two basic architectures: encoder-decoder architectures and two-pathway architectures.

1) *Encoder-decoder Architecture*: Compared to those methods with dilated convolutions, encoder-decoder architectures intuitively cost less computation and inference time. An encoder is usually a deep network with repeated spatial reduction to extract contextual information and the decoder restores the resolution to accomplish dense prediction by interpolation or transposed convolution [29]. Specially, an encoder can be a light-weight backbone pre-trained on ImageNet or an efficient variant designed based on it like ERFNet [5] and ESPNet [18]. Thus, the typical output resolution of an encoder is 1/32 of the input resolution. After processed by an encoder, resolution is gradually restored to 1/4 or 1/8 by upsampling modules and combining low-level information of the encoder.

2) *Two-pathway Architecture*: While the encoder-decoder architecture greatly reduces computation, it damages the performance of semantic segmentation because partial information is lost during the process of repeated downsampling and can not be restored by unsampling. Two-pathway architecture is proposed in order to alleviate this problem [21]. Besides one pathway of common encoders obtaining semantic information, the other shallow pathway of high resolution provides rich spatial details as a supplement. In order to achieve a good balance between accuracy and speed, the two pathways can be a light-weight encoder of sufficient depth and a shallow but wide branch made up of a few convolutions [26] [30]. The two pathways in BiSeNet are separated at the beginning while two branches in Fast-SCNN [22] share the learning to downsample module. Different from existing two-pathway methods, our DDRNet is implemented with two deep branches which share the early stages and exchange information with each other. The detailed differences are discussed in Section IV.

3) *Light-weight Encoder*: There are many computationally efficient backbones can be used as the encoder such as MobileNet [31], ShuffleNet [32] and small version of Xception [33]. MobileNet replaces standard convolutions with depth-

wise separable convolutions to low the number of parameters and computation. Strong regularization effect of depthwise separable convolutions is alleviated by inverted residual blocks in MobileNetV2 [34]. ShuffleNet utilizes the compactness of grouped convolutions and proposes a channel shuffle operation to promote information fusion between different groups. But all of these networks contain numerous depthwise separable convolutions which can not be implemented efficiently with existing GPU architecture. For this reason, though the FLOPs of ResNet-18 [28] is about six times of MobileNetV2 1.0 $\times$ , inference speed of ResNet-18 is higher than MobileNetV2 1.0 $\times$  on single 1080Ti GPU [23]. Thus, we employ numerous basic residual modules which comprise two sequential 3 $\times$ 3 convolutions and residual learning to build the whole network.

### C. Context Extraction Module

Another key point of semantic segmentation is how to capture more abundant contextual information. Atrous Spatial Pyramid Pooling (ASPP) [9] consists of parallel atrous convolution layers with different rates which can attend to multi-scale context information. Compared to ASPP, Pyramid Pooling Module (PPM) [11] in PSPNet is more computationally efficient by implementing pyramid pooling ahead of convolutional layers. Different from the local nature of convolutional kernels, self-attention mechanism is good at capturing global dependencies. In this way, Dual Attention Network (DANet) [35] takes advantage of both position attention and channel attention to further improve feature representation. Object Context Network (OCNet) [36] utilizes self-attention mechanism to explore object context which is defined as a set of pixels that belong to the same object category. Authors in CCNet [37] propose criss-cross attention to improve the efficiency of GPU memory and computation for non-local attention and apply it to semantic segmentation. In this paper, we do not make use of self-attention mechanism to capture context prior in view of its influence on inference speed. In contrast, we strengthen the PPM module with more scales and deep feature aggregation, and append it to the end of the low-resolution branch.

### III. METHOD

Firstly, we rethink the HRNet and analyze the key point of its superiority. Next, the whole pipeline was described, which consists of two parts: pre-training a dual-resolution classification backbone and applying it on the semantic segmentation dataset. We will introduce how to construct a dual-resolution network for classification and how to modify it to achieve superior performance on semantic segmentation tasks.

#### A. Rethinking HRNet

HRNet is a general architecture which maintains high-resolution representation throughout the whole network. In order to enhance model capacity, it starts from a high-resolution subnetwork as the first stage and high-to-low resolution subnetworks are added one by one to form more stages. So for the HRNet, there are actually several parallel multi-resolution branches and each branch is interconnected. Such complicate architecture enables HRNet to better extract features under different resolutions. From the results in [14], HRNet outperforms FPN-based ResNet on object detection, showing itself nature of multi-scale representation. HRNet also achieves better performance with much lower computation complexity and costs less inference time compared to DeepLabv3plus.

Learning from previous works, semantic segmentation demands high-resolution feature maps to be competent for dense prediction and large receptive fields to parse the scenes. By contrast, multi-scale representation ability is more significant for object detection tasks because neural network is supposed to detect as many multi-scale objects as possible in one image. From this point, the architecture of HRNet can be simplified through only reserving two branches. One branch is responsible for maintaining high-resolution feature maps while the other branch generates large enough receptive fields by repeated downsampling. We prove that such compact architecture can greatly improve the inference speed and reduce the memory consumption which is terrible for HRNet by extensive experiments.

#### B. Dual-resolution Network for Image Classification

For convenience, we can add an extra high-resolution branch on the widely used classification backbone such as ResNets. To get a trade-off between resolution and inference speed, we let the high-resolution branch create feature maps whose resolution is 1/8 of the input image resolution. Therefore, the extra branch is inserted following the end of the conv3 stage. Note that the extra branch does not contain any downsampling operation and has one-to-one correspondence with the original branch (low-resolution branch) to form deep high-resolution representation. Following HRNet, similar bridges are added between two pathways to perform bilateral feature fusion. The specific architectures of three dual-resolution networks with different parameters and GFLOPs are shown in Table I and Table II, where DDRNet-23 is derived from ResNet-18 and DDRNet-39 is derived from ResNet-34.

We modify the input stem of original ResNet, replacing one  $7\times 7$  convolutional layer with two sequential  $3\times 3$  convolutional layers. And then, basic residual blocks are utilized to

construct two branches. To enhance the representation ability, one bottleneck block is added at the end of each branch. The bilateral fusion includes fusing the high-resolution branch into the low-resolution branch (high-to-low fusion) and fusing the low-resolution into the high-resolution branch (low-to-high fusion). For the high-to-low fusion, high-resolution feature maps are downsampled by a sequence of  $3\times 3$  convolutions with a stride of 2 before pointwise summation. For the low-to-high resolution, low-resolution feature maps are firstly compressed by a  $1\times 1$  convolution and then upsampled by bilinear interpolation. Fig. 3 shows how bilateral fusion is implement. The  $i$ -th high-resolution feature map  $X_{Hi}$  and low-resolution feature map  $X_{Li}$  can be written as:

$$\begin{cases} X_{Hi} = R(F_H(X_{H(i-1)}) + T_{L-H}(F_L(X_{L(i-1)}))) \\ X_{Li} = R(F_L(X_{L(i-1)}) + T_{H-L}(F_H(X_{H(i-1)}))) \end{cases} \quad (1)$$

where  $F_H$  and  $F_L$  correspond to the sequence of basic residual blocks under high resolution and low resolution,  $T_{L-H}$  and  $T_{H-L}$  refer to the low-to-high and high-to-low transformer,  $R$  denotes the ReLU function.

The dual-resolution networks are trained on ImageNet [38] following the same data augmentation strategy as previous works [28], [39]. All the models are trained with input resolution of  $224\times 224$ , a batch size of 256 and 100 epoches on four 2080Ti GPUs. The initial learning rate is set to 0.1 and is reduced by 10 times at epoch 30, 60 and 90. We train all the networks using SGD with a weight decay of 0.0001 and a Nesterov momentum of 0.9. Top-1 errors on ImageNet validation set are shown in Table III. Though the efficiency of DDRNets is not superior to many advanced light backbones which are elaborately designed on ImageNet, our method still achieves start-of-the-art results on semantic segmentation dataset considering a speed trade-off. If combined with more powerful modules like [40] or attention mechanism [41], or architecture search [42], stronger pre-trained models can further boost performances on semantic segmentation with our method.

#### C. Deep Aggregation Pyramid Pooling Module

Here, a novel context extraction module named DAPPM is proposed, which can be seen as a combination of deep feature aggregation and pyramid pooling. Fig. 5 shows the interior structure of a DAPPM. Following MSFNet [24], we perform large pooling kernels and exponential strides to generate feature maps of 1/128, 1/256, 1/512 input image resolution. Input feature maps of 1/64 resolution and image-level information generated by global average pooling are also utilized. We believe that it is insufficient to blend all the multi-scale contextual information by single  $3\times 3$  or  $1\times 1$  convolution such as Pyramid Pooling Module. Inspired from Res2Net [40], we first upsample the feature maps and then fuse contextual information of different scales in a hierarchical-residual way followed by  $3\times 3$  convolutions. Considering an

TABLE I  
THE ARCHITECTURES OF DDRNET-23-SLIM AND DDRNET-23 FOR IMAGENET

stage	output	DDRNet-23-slim		DDRNet-23	
conv1	$112 \times 112$	$3 \times 3, 32, \text{stride } 2$		$3 \times 3, 64, \text{stride } 2$	
conv2	$56 \times 56$	$3 \times 3, 32, \text{stride } 2$		$3 \times 3, 64, \text{stride } 2$	
		$\begin{bmatrix} 3 \times 3, 32 \\ 3 \times 3, 32 \end{bmatrix} \times 2$		$\begin{bmatrix} 3 \times 3, 64 \\ 3 \times 3, 64 \end{bmatrix} \times 2$	
conv3	$28 \times 28$	$\begin{bmatrix} 3 \times 3, 64 \\ 3 \times 3, 64 \end{bmatrix} \times 2$		$\begin{bmatrix} 3 \times 3, 128 \\ 3 \times 3, 128 \end{bmatrix} \times 2$	
conv4	$14 \times 14, 28 \times 28$	$\begin{bmatrix} 3 \times 3, 128 \\ 3 \times 3, 128 \end{bmatrix} \times 2$	$\begin{bmatrix} 3 \times 3, 64 \\ 3 \times 3, 64 \end{bmatrix} \times 2$	$\begin{bmatrix} 3 \times 3, 256 \\ 3 \times 3, 256 \end{bmatrix} \times 2$	$\begin{bmatrix} 3 \times 3, 128 \\ 3 \times 3, 128 \end{bmatrix} \times 2$
		Bilateral fusion		Bilateral fusion	
conv5_1	$7 \times 7, 28 \times 28$	$\begin{bmatrix} 3 \times 3, 256 \\ 3 \times 3, 256 \end{bmatrix} \times 2$	$\begin{bmatrix} 3 \times 3, 64 \\ 3 \times 3, 64 \end{bmatrix} \times 2$	$\begin{bmatrix} 3 \times 3, 512 \\ 3 \times 3, 512 \end{bmatrix} \times 2$	$\begin{bmatrix} 3 \times 3, 128 \\ 3 \times 3, 128 \end{bmatrix} \times 2$
		Bilateral fusion		Bilateral fusion	
		$\begin{bmatrix} 1 \times 1, 256 \\ 3 \times 3, 256 \\ 1 \times 1, 512 \end{bmatrix} \times 1$	$\begin{bmatrix} 1 \times 1, 64 \\ 3 \times 3, 64 \\ 1 \times 1, 128 \end{bmatrix} \times 1$	$\begin{bmatrix} 1 \times 1, 512 \\ 3 \times 3, 512 \\ 1 \times 1, 1024 \end{bmatrix} \times 1$	$\begin{bmatrix} 1 \times 1, 128 \\ 3 \times 3, 128 \\ 1 \times 1, 256 \end{bmatrix} \times 1$
conv5_2	$7 \times 7$	High-to-low fusion		High-to-low fusion	
		$1 \times 1, 1024$		$1 \times 1, 2048$	
	$1 \times 1$	$7 \times 7$ global average pool		$7 \times 7$ global average pool	
		1000-d fc, softmax		1000-d fc, softmax	

TABLE II  
DDRNET-39 ARCHITECTURE FOR IMAGENET

stage	DDRNet-39
conv1	$3 \times 3, 64, \text{stride } 2$
conv2	$3 \times 3, 64, \text{stride } 2$
	$\begin{bmatrix} 3 \times 3, 64 \\ 3 \times 3, 64 \end{bmatrix} \times 3$
conv3	$\begin{bmatrix} 3 \times 3, 128 \\ 3 \times 3, 128 \end{bmatrix} \times 4$
conv4	$\begin{bmatrix} 3 \times 3, 256 \\ 3 \times 3, 256 \end{bmatrix} \times 3$
	Bilateral fusion
	$\begin{bmatrix} 3 \times 3, 128 \\ 3 \times 3, 128 \end{bmatrix} \times 3$
	Bilateral fusion
conv5_1	$\begin{bmatrix} 3 \times 3, 512 \\ 3 \times 3, 512 \end{bmatrix} \times 3$
	Bilateral fusion
	$\begin{bmatrix} 1 \times 1, 512 \\ 3 \times 3, 512 \\ 1 \times 1, 1024 \end{bmatrix} \times 1$
conv5_2	High-to-low fusion
	$1 \times 1, 2048$
	$7 \times 7$ global average pool
	1000-d fc, softmax

TABLE III  
TOP-1 ERROR RATES, PARAMETER SIZE AND GFLOPS OF THREE SCALED-UP DDRNETS

Model	top-1 err.	Params.	GFLOPs
DDRNet-23-slim	29.8	7.57M	0.98G
DDRNet-23	24.1	28.22M	3.88G
DDRNet-39	22.7	40.13M	6.95G

input  $x$ , each scale  $y_i$  can be written as:

$$y_i = \begin{cases} C_{1 \times 1}(x), & i = 1; \\ C_{3 \times 3}(U(C_{1 \times 1}(P_{2^{i+1}, 2^{i-1}}(x))) + y_{i-1}), & 1 < i < n; \\ C_{3 \times 3}(U(C_{1 \times 1}(P_{global}(x))) + y_{i-1}), & i = n. \end{cases} \quad (2)$$

where  $C_{1 \times 1}$  is  $1 \times 1$  convolution,  $C_{3 \times 3}$  is  $3 \times 3$  convolution,  $U$  denotes upsampling operation,  $P_{j,k}$  denotes the pool layer of which kernel size is  $j$  and stride is  $k$ ,  $P_{global}$  denotes the global average pooling. In the end, a  $1 \times 1$  convolution is performed to compress all the feature maps. Besides, a  $1 \times 1$  projection shortcut is added for easy optimization. Similar to SPP in SwiftNet [23], DAPPM is performed with the sequence BN-ReLU-Conv.

Inside a DAPPM, context extracted by larger pooling kernels is integrated with deeper information flow and multi-scale nature is formed by integrating different depth with different sizes of pooling kernel. Table IV shows that DAPPM is able to provide much richer context than PPM. Though DAPPM consists of more convolution layers and more complicate fusion, it hardly affects the inference speed because

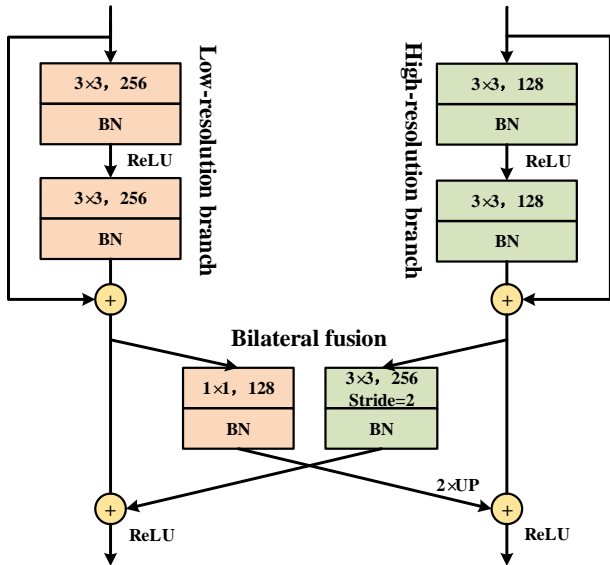


Fig. 3. The details of bilateral fusion in DDRNet. Summation fusion is implemented before ReLU.

TABLE IV  
CONSIDERING AN INPUT IMAGE OF  $1024 \times 1024$ , THE GENERATED  
CONTEXT SIZES OF PPM AND DAPPM ARE LISTED

	PPM	DAPPM
Output scale	[16, 6, 3, 2, 1]	[16] [16, 8] [16, 8, 4] [16, 8, 4, 2] [16, 8, 4, 2, 1]

itself input resolution is only 1/64 of input image resolution. Taking  $1024 \times 1024$  input for example, the maximum feature resolution of DAPPM is  $16 \times 16$ .

#### D. Overall Architecture for Semantic Segmentation

Fig. 4 shows the overview of our method. Some changes are made on DDRNet to achieve better performance on semantic segmentation task. First, the stride of  $3 \times 3$  convolution in the RBB of low-resolution branch is set to 2 to further downsample. And then, a DAPPM is added at the output of low-resolution branch, harvesting rich contextual information based on high-level feature maps of 1/64 resolution. Besides, the last high-to-low fusion is replaced with low-to-high fusion which is implemented with bilinear interpolation and summation fusion. At last, we devise a simple segmentation head which consists of one  $3 \times 3$  convolutional layer followed by one  $1 \times 1$  convolutional layer. Computational load of the segmentation head can be adjusted by changing output dimension of the  $3 \times 3$  convolutional layer. We set the value to 64 for DDRNet-23-slim, 128 for DDRNet-23 and 256 for DDRNet-39. Note that except the segmentation head and the DAPPM module, all the modules have been pre-trained on ImageNet.

#### E. Deep Supervision

Extra supervisions during training stage can ease the optimization of deep convolutional neural networks (DCNNs). In PSPNet, an auxiliary loss is added at the output of res4\_22 block of ResNet-101 and the corresponding weight is set to 0.4 according to experimental results [11]. BiSeNetV2 [26] proposes a booster training strategy in which extra segmentation heads are added at the end of each stage of the semantic branch. However, it needs a number of experiments to find the optimal weights which are used to balance each loss, and leads to a non-negligible increase in training memory. In order to acquire better results, SFNet [43] utilizes a similar strategy named Cascaded Deeply Supervised Learning. In this paper, we only report results obtained by adopting single extra supervision for fair comparison with most of the methods. We add an auxiliary loss as shown in Fig. 4 and set the weight to 0.4 following PSPNet. The auxiliary segmentation head can be discarded in the testing stage. The final loss which is sum of cross-entropy can be expressed as:

$$L_f = L_n + \alpha L_a \quad (3)$$

where  $L_f, L_n, L_a$  represents the final loss, normal loss, auxiliary loss respectively and  $\alpha$  denotes the weight of auxiliary loss, which is 0.4 in this paper.

#### IV. DIFFERENCES BETWEEN OUR METHOD AND OTHER BILATERAL NETWORKS

Bilateral Segmentation Network (BiSeNet) devises two branches to learn spatial information and context information separately [21]. Its authors claim that the detail branch, namely high-resolution branch, should be shallow and wide for faster inference speed. According to results in BiSeNetV2 [26], though deeper model with less GFLOPs outperforms wider model, performance starts to degrade when network depth is scaled up to critical value. We think that it should be ascribed to the absence of residual learning and efficient supervision because most semantic segmentation datasets equip fewer finely annotated images compared to classification datasets. BiSeNetV2 works well in extremely real-time scenarios but difficult to be applied to high-accuracy segmentation models.

Fast-SCNN is another excellent method which utilizes two branches to speed semantic segmentation [22]. Different from BiSeNet, its two branches share the first three convolution blocks for learning downsampling. But similar to BiSeNet, the high-resolution branch of Fast-SCNN is very shallow because it only uses one high-resolution convolutional layer to process the output from learning to downsample module.

Similar to Fast-SCNN, the two branches share the first several stages in DDRNet. But after that there are one-by-one corresponding relations between the high-resolution branch and the low-resolution branch. DDRNet allows more information exchange and generates high-resolution feature maps with large enough receptive fields which we think have a greatly positive influence on semantic segmentation. Besides, we first pre-train the dual-resolution network on ImageNet dataset before training it on semantic segmentation dataset, while most two-pathway methods do not fully benefit from ImageNet

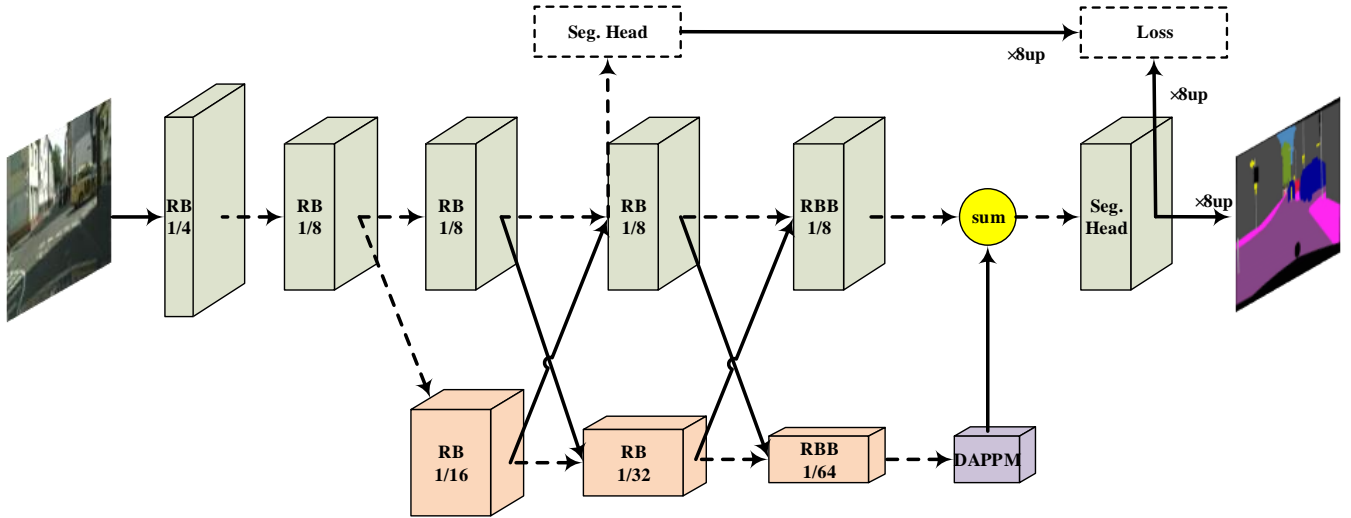


Fig. 4. The overview of DDRNets on semantic segmentation. “RB” denotes sequential residual basic blocks. “RBB” denotes single residual bottleneck block. “DAPPM” denotes the Deep Aggregation Pyramid Pooling Module. “Seg. Head” denotes the segmentation head. Black solid lines denote information paths with data processing (including upsampling and downsampling) and black dashed lines denote information path without data processing. “sum” denotes pointwise concatenation. Dashed boxes denote the components which are disregarded in the inference stage.

## V. EXPERIMENTS

### A. Datasets

Cityscapes [44] is one of the most famous datasets focusing on urban street scenes parsing. The dataset contains 2975 finely annotated images for training, 500 images for validation and 1525 images for test. We do not use extra 20000 coarsely labeled images during train. There are total 19 classes available for semantic segmentation task. The resolution of images is  $2048 \times 1024$  which is consistent with self-driving requirements but challenging to achieve the real-time inference.

CamVid [45] consists of 701 densely annotated frames and resolution of each frame is  $960 \times 720$ . We split it into 367 for training, 101 for validation and 233 for test following previous works. We merge train set and validation set at actual train and evaluate our models on test set using 11 classes.

### B. Train Setting

1) *Cityscapes*: Following [50], we use the SGD optimizer with the initial learning rate of 0.01, the momentum of 0.9 and the weight decay of 0.0005. We adopt the ploy learning policy with the power of 0.9 to drop the learning rate and implement the data augmented method including random cropping images, random scaling in the range of 0.5 to 2.0 and random horizontal flipping. Images are randomly cropped into  $1024 \times 1024$  for training following [20], [24], [43]. All the models are trained with 484 epoches (about 120K iterations), a batch size of 12 and using syncBN on four 2080Ti GPUs. Before evaluating on test server, we use images from train and val set at the same time for local training. For fair comparison with [26] and [43], online hard example mining (OHEM) [51] is also used.

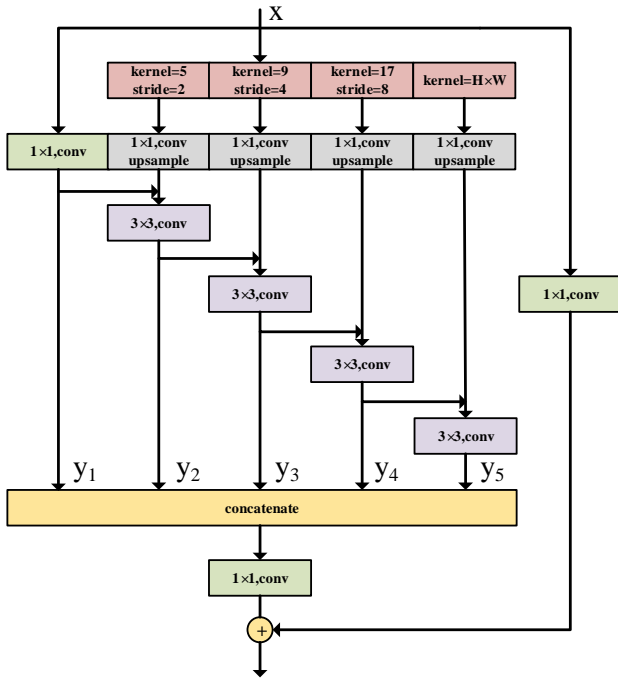


Fig. 5. The detailed architecture of Deep Aggregation Pyramid Pooling Module. The number of multi-scale branches can be adjusted according to input resolution.

pre-training. Though our method is proposed for real-time segmentation, it is equipped to compete with methods designed for pure pursuit of accuracy.

TABLE V

ACCURACY AND SPEED COMPARISON ON CITYSCAPES. WE REPORT RESULTS ON BOTH VAL SET AND TEST SET. SINCE INFERENCE SPEED OF DIFFERENT MODELS IS MEASURED UNDER DIFFERENT CONDITIONS, THE CORRESPONDING GPU MODELS AND INPUT RESOLUTIONS ARE REPORTED. OUR GFLOPS CALCULATION ADOPTS  $2048 \times 1024$  IMAGE AS INPUT. THE CORRESPONDING SPEED IS MEASURED USING TENSORRT ACCELERATION IF THE METHOD IS MARKED WITH †

Model	MIoU		Speed (FPS)	GPU	Resolution	GFLOPs	Params
	val	test					
SegNet [46]	-	57	16.7	TitanX	$640 \times 360$	286	29.5M
ENet [15]	-	57	135.4	TitanX	$640 \times 360$	3.8	0.4M
SQ [47]	-	59.8	16.7	TitanX	$2048 \times 1024$	270	-
ICNet [17]	-	69.5	30	TitanX M	$2048 \times 1024$	28.3	26.5M
ESPNet [18]	-	60.3	113	TitanX	$1024 \times 512$	-	0.4M
ERFNet [5]	70.0	68.0	41.7	TitanX M	$1024 \times 512$	27.7	20M
Fast-SCNN [22]	68.6	68.0	123.5	TitanXp	$2048 \times 1024$	-	1.1M
DFANet A [20]	-	71.3	100	TitanX	$1024 \times 1024$	3.4	7.8M
DFANet B [20]	-	67.1	120	TitanX	$1024 \times 1024$	2.1	4.8M
SwiftNetRN-18 [23]	75.5	75.4	39.9	GTX 1080Ti	$2048 \times 1024$	104.0	11.8M
SwiftNetRN-18 ens [23]	-	76.5	18.4	GTX 1080Ti	$2048 \times 1024$	218.0	24.7M
BiSeNet1 [21]	69.0	68.4	105.8	GTX 1080Ti	$1536 \times 768$	14.8	5.8M
BiSeNet2 [21]	74.8	74.7	65.5	GTX 1080Ti	$1536 \times 768$	55.3	49M
BiSeNetV2† [26]	73.4	72.6	<b>156</b>	GTX 1080Ti	$1024 \times 512$	21.1	-
BiSeNetV2-L† [26]	75.8	75.3	47.3	GTX 1080Ti	$1024 \times 512$	118.5	-
CAS [48]	71.6	70.5	108	TitanXp	$1536 \times 768$	-	-
GAS [49]	72.4	71.8	108.4	TitanXp	$1537 \times 769$	-	-
SFNet(DF1) [43]	-	74.5	74	GTX 1080Ti	$2048 \times 1024$	-	9.03M
SFNet(DF2) [43]	-	77.8	53	GTX 1080Ti	$2048 \times 1024$	-	10.53M
SFNet(ResNet-18) [43]	-	78.9	18	GTX 1080Ti	$2048 \times 1024$	247	12.87M
MSFNet* [24]	-	71.3	117	GTX 2080Ti	$1024 \times 512$	24.2	-
MSFNet [24]	-	77.1	41	GTX 2080Ti	$2048 \times 1024$	96.8	-
CABiNet [30]	76.6	75.9	76.5	GTX 2080Ti	$2048 \times 1024$	12.0	2.64M
DDRNet-23-Slim	<b>77.8</b>	77.4	108.8	GTX 2080Ti	$2048 \times 1024$	36.3	5.7M
DDRNet-23	<b>79.5</b>	79.4	38.5	GTX 2080Ti	$2048 \times 1024$	143.1	20.1M
DDRNet-39	-	<b>80.4</b>	22.7	GTX 2080Ti	$2048 \times 1024$	281.2	32.3M

2) *CamVid*: We set the initial learning rate to 0.001 and train all the models for 968 epoches. Images are randomly cropped into  $960 \times 720$  for training following [20]. All the models are trained on single GPU and other training details are identical to those for Cityscapes. When employing Cityscapes pre-train, we fine-tune the models for 200 epoches with the initial learning rate of 0.001.

### C. Measure of Inference Speed

The inference speed is measured on a single GTX 2080Ti GPU by setting the batch size to 1 and with CUDA 10.0, CUDNN 7.6 and PyTorch 1.3. We follow the test code provided by SwiftNet [23] for accurate measurement. Similar to MSFNet and SwiftNet, we exclude batch normalization layers after convolutional layers because they can be integrated into convolutions during inference. We run the same network 500 times under input resolution of  $2048 \times 1024$  for Cityscapes and input resolution of  $960 \times 720$  for CamVid, and report the average time to eliminate occasionality.

### D. Speed and Accuracy Comparisons

1) *Cityscapes*: As can be observed from Table V and Fig. 1, our method achieves a new state-of-the-art trade-off between real-time and high-accuracy. Specially, DDRNet-23-slim (our smallest model) achieves 77.4% mIoU on test set

at 109 FPS. It outperforms DFANet A and MSFNet (under  $1024 \times 512$ ) by 6.1% test mIoU with similar inference speed, and reasons approximate three times as fast as MSFNet under same resolution. Besides, it runs 50% faster than the smallest SFNet and achieves 2.9% mIoU gain on test set. It is worth noting that our method also towers over those methods based on architecture search for real-time semantic segmentation including CAS [48] and GAS [49] at a similar inference speed. For wider models, DDRNet-23 achieves the overall best accuracy among the existing real-time methods, reaching 79.4% mIoU at 39 FPS. DDRNet-23 has the performance gain of 0.5% over SFNet (ResNet-18) but runs much faster than it. We keep going deeper and wider with DDRNets, achieving 80.4% mIoU on Cityscapes test server at 23 FPS, only using fine annotated data. If combined with pre-training on much bigger dataset and TensorRT acceleration like [43], our method can build a skyscraping baseline for real-time semantic segmentation of road scenes. On Cityscapes val set, DDRNet-23-slim outperforms all published results of real-time methods with 36.3 GFLOPs and 5.7M parameters. And DDRNet-23 achieves a new overall best result of 79.5% mIoU. Fig. 6 shows the visilized results of DDRNet-23-slim and DDRNet-23 under different scenes.

2) *CamVid*: As shown in Table VI, DDRNet-23-slim achieves 74.4% mIoU on CamVid test set at 230 FPS without

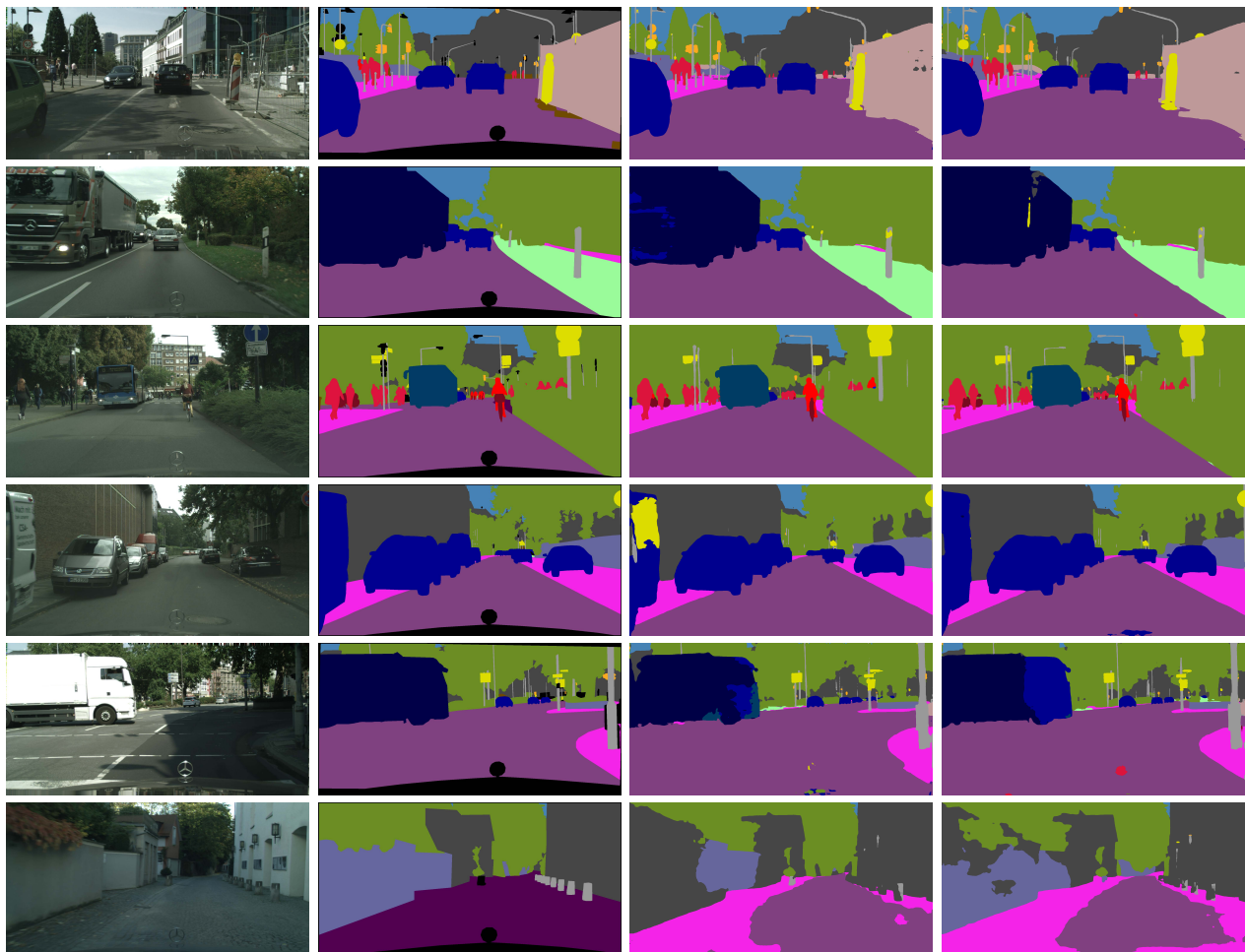


Fig. 6. Visualized segmentation results on Cityscapes val set. The four columns left-to-right refer to input image, ground truth, the output of DDRNet-23-slim, and the output of DDRNet-23. The first four rows show the performance of two models while the last two rows represent some segmentation failures.

Cityscapes pre-train. It obtains the second-highest accuracy and runs faster than all the other methods. In the meanwhile, the performance of DDRNet-23 is better than previous state-of-the-art method MSFNet. DDRNet-23 also has a big performance gain over BiSeNetV2-L and SFNet (ResNet-18) but runs about two times faster than them. Given that training pixels of CamVid are much less than that of Cityscapes, we believe that the outstanding performances of DDRNets partly attribute to appropriate ImageNet pre-training. In addition, our models pre-trained on Cityscapes achieve superior segmentation accuracy at the real-time inference speed. Specially, Cityscapes pre-trained DDRNet-23 realizes 79.9% mIoU at 94 FPS, stronger and much faster than BiSeNetV2-L.

### E. Comparisons with State-of-the-art Results

In this part, we further demonstrate the capacity of DDRNet for semantic segmentation by comparing to state-of-the-art models on Cityscapes test set. Such methods frequently perform multi-scale and horizontal flip inference to achieve better results regardless of time cost. For fair comparison with them, we also apply multiple scales including  $0.50\times$ ,  $0.75\times$ ,  $1\times$ ,  $1.25\times$ ,  $1.5\times$ ,  $1.75\times$ ,  $2\times$  with left-right flipping during test. As is shown in Table VII, standard test augmentation improves

the accuracy of DDRNet-39 from 80.4% to 81.9%. Besides, DDRNet-39 outperforms numerous powerful models which are integrated with self-attention modules including CCNet, DANet and OCNet. It is noteworthy that our method only requires 11% computation of DANet. DDRNet-39 also gets ahead of SFNet (based on ResNet-101 backbone) which is a state-of-the-art method for real-time semantic segmentation, only requiring 34% computation. DDRNet-39  $1.5\times$  of which size is closer to other models in Table VII is a wider version of DDRNet-39, achieving a very competitive performance of 82.4% mIoU.

### F. Comparisons with HRNet

The most difference between DDRNet and HRNet is the number of parallel branches. Besides, we apply the multi-scale context extraction module to features maps of very low resolution. Experimental results in Table VIII demonstrate the great improvement of DDRNet over HRNet in both inference time and train memory usage. We get the val results of two small HRNets from official implementation on Github. Training memory is measured by deploying the models with a batch size of 2 on single 2080Ti at a crop size of  $1024\times 512$ , and excluding the auxiliary segmentation head.

TABLE VI

ACCURACY AND SPEED COMPARISON ON CAMVID TEST SET. MSFNET RUNS AT  $1024 \times 768$  AND MSFNET\* RUNS AT  $768 \times 512$  WHILE OTHER METHODS RUN AT  $960 \times 720$ . THE CORRESPONDING SPEED IS MEASURED USING TENSORRT ACCELERATION IF THE METHOD IS MARKED WITH †.

Model	mIoU	Speed (FPS)	GPU
w/o Cityscapes pre-train			
DFANet A [20]	64.7	120	TitanX
DFANet B [20]	59.3	160	TitanX
SwiftNetRN-18 pyr [23]	73.9	-	GTX 1080Ti
SwiftNetRN-18 [23]	72.6	-	GTX 1080Ti
BiSeNet1 [21]	65.6	175	GTX 1080Ti
BiSeNet2 [21]	68.7	116	GTX 1080Ti
BiSeNetV2† [26]	72.4	124	GTX 1080Ti
BiSeNetV2-L† [26]	73.2	33	GTX 1080Ti
CAS [48]	71.2	169	TitanXp
GAS [49]	72.8	153	TitanXp
SFNet(DF2) [43]	70.4	134	GTX 1080Ti
SFNet(ResNet-18) [43]	73.8	36	GTX 1080Ti
MSFNet* [24]	72.7	160	GTX 2080Ti
MSFNet [24]	75.4	91	GTX 2080Ti
DDRNet-23-slim	74.4	<b>230</b>	GTX 2080Ti
DDRNet-23	<b>76.3</b>	94	GTX 2080Ti
w/ Cityscapes pre-train			
VideoGCRF [52]	75.2	-	-
CCNet3D [53]	79.1	-	-
BiSeNetV2† [26]	76.7	124	GTX 1080Ti
BiSeNetV2-L† [26]	78.5	33	GTX 1080Ti
DDRNet-23-slim	78.0	<b>230</b>	GTX 2080Ti
DDRNet-23	<b>79.9</b>	94	GTX 2080Ti

TABLE VII

STATE-OF-THE-ART MODELS ON CITYSCAPES TEST SET. OS DENOTES THE FINAL OUTPUT STRIDE. ALL THE METHODS TRAIN MODELS ON BOTH TRAIN AND VAL SET EXCEPT PSPNET MARKED WITH † ONLY USING TRAIN SET. GFLOPS CALCULATION ADOPTS  $1024 \times 1024$  IMAGE AS INPUT AND MOST OF RESULTS ABOUT GFLOPS AND PARAMS CAN BE FOUND IN [43]

Model	OS	mIoU	GFLOPs	Params.
SAC [54]	8	78.1	-	-
DepthSeg [55]	8	78.2	-	-
PSPNet† [11]	8	78.4	1065.4	65.7M
ResNet38 [56]	8	78.4	-	-
BiSeNet [21]	8	78.9	219.1	51.0M
DFN [57]	8	79.3	1121.0	90.7M
PSANet [58]	8	80.1	1182.6	85.6M
DenseASPP [12]	8	80.6	632.9	35.7M
CCNet [37]	8	81.4	1153.9	66.5M
DANet [35]	8	81.5	1298.8	66.6M
OCNet [36]	8	81.7	-	-
OCRNet [59]	8	81.8	-	-
HRNetV2-W48 [50]	4	81.6	348.1	65.9M
SFNet [43]	4	81.8	417.5	50.3M
DDRNet-39	8	81.9	<b>140.6</b>	<b>32.3M</b>
DDRNet-39 1.5×	8	<b>82.4</b>	303.0	70.2M

TABLE VIII

COMPARATIVE EXPERIMENTS BETWEEN DDRNET AND HRNET IN TERMS OF MIOU, FPS AND TRAIN MEMORY

Model	mIoU	FPS	Train mem.
HRNetV2-W18-Small-v1 [50]	70.3	72.0	1989MiB
HRNetV2-W18-Small-v2 [50]	76.2	32.3	2745MiB
DDRNet-23-slim	<b>76.9</b>	<b>108.8</b>	<b>1629MiB</b>

TABLE IX

INFLUENCES OF STANDARD BELLS AND WHISTLES, INCLUDING DEEP SUPERVISION (DS), OHEM AND TRAIN AT A CROP SIZE OF  $1024 \times 1024$

Model	DS	OHEM	$1024 \times 1024$	mIoU
DDRNet-23-slim				76.1
DDRNet-23-slim	✓			76.1
DDRNet-23-slim	✓	✓		76.9
DDRNet-23-slim	✓	✓	✓	77.8

TABLE X

ANALYSIS OF PPM AND DAPPM ON ACCURACY AND SPEED.

Model	PPM	DAPPM	mIoU	Speed
DDRNet-23-slim			74.1	115.3
DDRNet-23-slim	✓		76.8	111.4
DDRNet-23-slim		✓	77.8	108.8

### G. Ablative Experiments on Cityscapes

1) *Ablative Experiment of Standard Bells and Whistles:* We analyze the effect of some basic training tricks which are also adopted by recent advanced method SFNet [43]. As shown in Table IX, the accuracy is raised from 76.1 to 77.8 with deep supervision, OHEM, and train at a larger crop size (the default is  $1024 \times 512$ ).

2) *Ablative Experiment of DAPPM:* In this part, the effectiveness of DAPPM is demonstrated by comparison with PPM which is a widely used global-context extractor. For fair comparison, we choose the SPP in SwiftNet which is a simplified version of PPM. The results in Table X suggest that context extraction modules can greatly improve the performance of scene parsing, from 74.1% mIoU to 77.8% mIoU. Benefited from extracting context on very low-resolution feature maps, inference speed is hardly affected. Besides, DAPPM achieves 1% mIoU gain compared to simplified PPM.

## VI. CONCLUSION

In this paper, a novel deep dual-resolution architecture is proposed for real-time semantic segmentation of road scenes and a new module for extracting multi-scale contextual information is presented. To our best knowledge, we are the first to introduce deep high-resolution representation into real-time semantic segmentation and our simple strategy outperforms all previous models on two popular benchmarks without any extra bells or whistles. Most existing real-time networks are elaborately designed or are advanced backbones specially devised for ImageNet, which are very different from dilated backbone widely used for high-accuracy methods. By contrast, DDRNet only utilizes basic residual modules and bottleneck modules, and can provide a wide range of speed and accuracy trade-off by scaling model width and depth. Due to the simplicity and efficiency of our method, it can be seen as a strong baseline towards unifying real-time and high-accuracy semantic segmentation.

## REFERENCES

- [1] Z. Liu, X. Li, P. Luo, C. C. Loy, and X. Tang, "Deep learning markov random field for semantic segmentation," *IEEE Transactions on Pattern Analysis and Machine Intelligence*, vol. 40, no. 8, pp. 1814–1828, 2018.
- [2] L. Jing, Y. Chen, and Y. Tian, "Coarse-to-fine semantic segmentation from image-level labels," *IEEE Transactions on Image Processing*, vol. 29, pp. 225–236, 2020.
- [3] X. Ren, S. Ahmad, L. Zhang, L. Xiang, D. Nie, F. Yang, Q. Wang, and D. Shen, "Task decomposition and synchronization for semantic biomedical image segmentation," *IEEE Transactions on Image Processing*, vol. 29, pp. 7497–7510, 2020.
- [4] M. Saha and C. Chakraborty, "Her2net: A deep framework for semantic segmentation and classification of cell membranes and nuclei in breast cancer evaluation," *IEEE Transactions on Image Processing*, vol. 27, no. 5, pp. 2189–2200, 2018.
- [5] E. Romera, J. M. Alvarez, L. M. Bergasa, and R. Arroyo, "Erfnet: Efficient residual factorized convnet for real-time semantic segmentation," *IEEE Transactions on Intelligent Transportation Systems*, vol. 19, no. 1, pp. 263–272, 2017.
- [6] J. Long, E. Shelhamer, and T. Darrell, "Fully convolutional networks for semantic segmentation," in *Proceedings of the IEEE Conference on Computer Vision and Pattern Recognition*, pp. 3431–3440, 2015.
- [7] L.-C. Chen, G. Papandreou, I. Kokkinos, K. Murphy, and A. L. Yuille, "Semantic image segmentation with deep convolutional nets and fully connected crfs," *arXiv preprint arXiv:1412.7062*, 2014.
- [8] S. Mallat, *A wavelet tour of signal processing*. Elsevier, 1999.
- [9] L.-C. Chen, G. Papandreou, I. Kokkinos, K. Murphy, and A. L. Yuille, "Deeplab: Semantic image segmentation with deep convolutional nets, atrous convolution, and fully connected crfs," *IEEE Transactions on Pattern Analysis and Machine Intelligence*, vol. 40, no. 4, pp. 834–848, 2017.
- [10] L.-C. Chen, G. Papandreou, F. Schroff, and H. Adam, "Rethinking atrous convolution for semantic image segmentation," *arXiv preprint arXiv:1706.05587*, 2017.
- [11] H. Zhao, J. Shi, X. Qi, X. Wang, and J. Jia, "Pyramid scene parsing network," in *Proceedings of the IEEE Conference on Computer Vision and Pattern Recognition*, pp. 2881–2890, 2017.
- [12] M. Yang, K. Yu, C. Zhang, Z. Li, and K. Yang, "Denseaspp for semantic segmentation in street scenes," in *Proceedings of the IEEE Conference on Computer Vision and Pattern Recognition*, pp. 3684–3692, 2018.
- [13] K. Sun, B. Xiao, D. Liu, and J. Wang, "Deep high-resolution representation learning for human pose estimation," in *Proceedings of the IEEE Conference on Computer Vision and Pattern Recognition*, pp. 5693–5703, 2019.
- [14] K. Sun, Y. Zhao, B. Jiang, T. Cheng, B. Xiao, D. Liu, Y. Mu, X. Wang, W. Liu, and J. Wang, "High-resolution representations for labeling pixels and regions," *arXiv preprint arXiv:1904.04514*, 2019.
- [15] A. Paszke, A. Chaurasia, S. Kim, and E. Culurciello, "Enet: A deep neural network architecture for real-time semantic segmentation," *arXiv preprint arXiv:1606.02147*, 2016.
- [16] Z. Yang, H. Yu, M. Feng, W. Sun, X. Lin, M. Sun, Z. H. Mao, and A. Mian, "Small object augmentation of urban scenes for real-time semantic segmentation," *IEEE Transactions on Image Processing*, vol. 29, pp. 5175–5190, 2020.
- [17] H. Zhao, X. Qi, X. Shen, J. Shi, and J. Jia, "Icnet for real-time semantic segmentation on high-resolution images," in *Proceedings of the European Conference on Computer Vision*, pp. 405–420, 2018.
- [18] S. Mehta, M. Rastegari, A. Caspi, L. Shapiro, and H. Hajishirzi, "Espnet: Efficient spatial pyramid of dilated convolutions for semantic segmentation," in *Proceedings of the European Conference on Computer Vision*, pp. 552–568, 2018.
- [19] B. Jiang, W. Tu, C. Yang, and J. Yuan, "Context-integrated and feature-refined network for lightweight object parsing," *IEEE Transactions on Image Processing*, vol. 29, pp. 5079–5093, 2020.
- [20] H. Li, P. Xiong, H. Fan, and J. Sun, "Dfanet: Deep feature aggregation for real-time semantic segmentation," in *Proceedings of the IEEE Conference on Computer Vision and Pattern Recognition*, pp. 9522–9531, 2019.
- [21] C. Yu, J. Wang, C. Peng, C. Gao, G. Yu, and N. Sang, "Bisenet: Bilateral segmentation network for real-time semantic segmentation," in *Proceedings of the European Conference on Computer Vision*, pp. 325–341, 2018.
- [22] R. P. Poudel, S. Liwicki, and R. Cipolla, "Fast-scnn: Fast semantic segmentation network," *arXiv preprint arXiv:1902.04502*, 2019.
- [23] M. Orsic, I. Kreso, P. Bevandic, and S. Segvic, "In defense of pre-trained imagenet architectures for real-time semantic segmentation of road-driving images," in *Proceedings of the IEEE Conference on Computer Vision and Pattern Recognition*, pp. 12607–12616, 2019.
- [24] H. Si, Z. Zhang, F. Lv, G. Yu, and F. Lu, "Real-time semantic segmentation via multiply spatial fusion network," *arXiv preprint arXiv:1911.07217*, 2019.
- [25] P. Hu, F. Perazzi, F. C. Heilbron, O. Wang, Z. Lin, K. Saenko, and S. Sclaroff, "Real-time semantic segmentation with fast attention," *arXiv preprint arXiv:2007.03815*, 2020.
- [26] C. Yu, C. Gao, J. Wang, G. Yu, C. Shen, and N. Sang, "Bisenet v2: Bilateral network with guided aggregation for real-time semantic segmentation," *arXiv preprint arXiv:2004.02147*, 2020.
- [27] L.-C. Chen, Y. Zhu, G. Papandreou, F. Schroff, and H. Adam, "Encoder-decoder with atrous separable convolution for semantic image segmentation," in *Proceedings of the European Conference on Computer Vision*, pp. 801–818, 2018.
- [28] K. He, X. Zhang, S. Ren, and J. Sun, "Deep residual learning for image recognition," in *Proceedings of the IEEE Conference on Computer Vision and Pattern Recognition*, pp. 770–778, 2016.
- [29] M. D. Zeiler, D. Krishnan, G. W. Taylor, and R. Fergus, "Deconvolutional networks," in *2010 IEEE Computer Society Conference on Computer Vision and Pattern Recognition*, pp. 2528–2535.
- [30] S. Kumar, Y. Lyu, F. Nex, and M. Y. Yang, "Cabinet: Efficient context aggregation network for low-latency semantic segmentation," *arXiv preprint arXiv:2011.00993*, 2020.
- [31] A. G. Howard, M. Zhu, B. Chen, D. Kalenichenko, W. Wang, T. Weyand, M. Andreetto, and H. Adam, "Mobilenets: Efficient convolutional neural networks for mobile vision applications," *arXiv preprint arXiv:1704.04861*, 2017.
- [32] X. Zhang, X. Zhou, M. Lin, and J. Sun, "Shufflenet: An extremely efficient convolutional neural network for mobile devices," in *Proceedings of the IEEE Conference on Computer Vision and Pattern Recognition*, pp. 6848–6856, 2018.
- [33] F. Chollet, "Xception: Deep learning with depthwise separable convolutions," in *Proceedings of the IEEE Conference on Computer Vision and Pattern Recognition*, pp. 1251–1258, 2017.
- [34] M. Sandler, A. Howard, M. Zhu, A. Zhmoginov, and L.-C. Chen, "Mobilenetv2: Inverted residuals and linear bottlenecks," in *Proceedings of the IEEE Conference on Computer Vision and Pattern Recognition*, pp. 4510–4520, 2018.
- [35] J. Fu, J. Liu, H. Tian, Y. Li, Y. Bao, Z. Fang, and H. Lu, "Dual attention network for scene segmentation," in *Proceedings of the IEEE Conference on Computer Vision and Pattern Recognition*, pp. 3146–3154, 2019.
- [36] Y. Yuan and J. Wang, "Ocnet: Object context network for scene parsing," *arXiv preprint arXiv:1809.00916*, 2018.
- [37] Z. Huang, X. Wang, L. Huang, C. Huang, Y. Wei, and W. Liu, "Ccnet: Criss-cross attention for semantic segmentation," in *Proceedings of the IEEE International Conference on Computer Vision*, pp. 603–612, 2019.
- [38] O. Russakovsky, J. Deng, H. Su, J. Krause, S. Satheesh, S. Ma, Z. Huang, A. Karpathy, A. Khosla, M. Bernstein, *et al.*, "Imagenet large scale visual recognition challenge," *International Journal of Computer Vision*, vol. 115, no. 3, pp. 211–252, 2015.
- [39] S. Xie, R. Girshick, P. Dollár, Z. Tu, and K. He, "Aggregated residual transformations for deep neural networks," in *Proceedings of the IEEE Conference on Computer Vision and Pattern Recognition*, pp. 1492–1500, 2017.
- [40] S. Gao, M.-M. Cheng, K. Zhao, X.-Y. Zhang, M.-H. Yang, and P. H. Torr, "Res2net: A new multi-scale backbone architecture," *IEEE Transactions on Pattern Analysis and Machine Intelligence*, 2019.
- [41] J. Hu, L. Shen, and G. Sun, "Squeeze-and-excitation networks," in *Proceedings of the IEEE Conference on Computer Vision and Pattern Recognition*, pp. 7132–7141, 2018.
- [42] A. Howard, M. Sandler, G. Chu, L.-C. Chen, B. Chen, M. Tan, W. Wang, Y. Zhu, R. Pang, V. Vasudevan, *et al.*, "Searching for mobilenetv3," in *Proceedings of the IEEE International Conference on Computer Vision*, pp. 1314–1324, 2019.
- [43] X. Li, A. You, Z. Zhu, H. Zhao, M. Yang, K. Yang, and Y. Tong, "Semantic flow for fast and accurate scene parsing," *arXiv preprint arXiv:2002.10120*, 2020.
- [44] M. Cordts, M. Omran, S. Ramos, T. Rehfeld, M. Enzweiler, R. Benenson, U. Franke, S. Roth, and B. Schiele, "The cityscapes dataset for semantic urban scene understanding," in *Proceedings of the IEEE Conference on Computer Vision and Pattern Recognition*, pp. 3213–3223, 2016.

- [45] G. J. Brostow, J. Fauqueur, and R. Cipolla, "Semantic object classes in video: A high-definition ground truth database," *Pattern Recognition Letters*, vol. 30, no. 2, pp. 88–97, 2009.
- [46] V. Badrinarayanan, A. Kendall, and R. Cipolla, "Segnet: A deep convolutional encoder-decoder architecture for image segmentation," *IEEE Transactions on Pattern Analysis and Machine Intelligence*, vol. 39, no. 12, pp. 2481–2495, 2017.
- [47] M. Treml, J. Arjona-Medina, T. Unterthiner, R. Durgesh, F. Friedmann, P. Schuberth, A. Mayr, M. Heusel, M. Hofmarcher, M. Widrich, *et al.*, "Speeding up semantic segmentation for autonomous driving," in *MLITS, NIPS Workshop*, vol. 2, 2016.
- [48] Y. Zhang, Z. Qiu, J. Liu, T. Yao, D. Liu, and T. Mei, "Customizable architecture search for semantic segmentation," in *Proceedings of the IEEE Conference on Computer Vision and Pattern Recognition*, pp. 11641–11650, 2019.
- [49] P. Lin, P. Sun, G. Cheng, S. Xie, X. Li, and J. Shi, "Graph-guided architecture search for real-time semantic segmentation," in *Proceedings of the IEEE/CVF Conference on Computer Vision and Pattern Recognition*, pp. 4203–4212, 2020.
- [50] J. Wang, K. Sun, T. Cheng, B. Jiang, C. Deng, Y. Zhao, D. Liu, Y. Mu, M. Tan, X. Wang, W. Liu, and B. Xiao, "Deep high-resolution representation learning for visual recognition," *IEEE Transactions on Pattern Analysis and Machine Intelligence*, pp. 1–1, 2020.
- [51] A. Shrivastava, A. Gupta, and R. Girshick, "Training region-based object detectors with online hard example mining," in *Proceedings of the IEEE Conference on Computer Vision and Pattern Recognition*, pp. 761–769, 2016.
- [52] S. Chandra, C. Couprie, and I. Kokkinos, "Deep spatio-temporal random fields for efficient video segmentation," in *Proceedings of the IEEE Conference on Computer Vision and Pattern Recognition*, pp. 8915–8924, 2018.
- [53] Z. Huang, X. Wang, Y. Wei, L. Huang, H. Shi, W. Liu, and T. S. Huang, "Ccnnet: Criss-cross attention for semantic segmentation," *IEEE Transactions on Pattern Analysis and Machine Intelligence*, pp. 1–1, 2020.
- [54] R. Zhang, S. Tang, Y. Zhang, J. Li, and S. Yan, "Scale-adaptive convolutions for scene parsing," in *Proceedings of the IEEE International Conference on Computer Vision*, pp. 2031–2039, 2017.
- [55] S. Kong and C. C. Fowlkes, "Recurrent scene parsing with perspective understanding in the loop," in *Proceedings of the IEEE Conference on Computer Vision and Pattern Recognition*, pp. 956–965, 2018.
- [56] Z. Wu, C. Shen, and A. Van Den Hengel, "Wider or deeper: Revisiting the resnet model for visual recognition," *Pattern Recognition*, vol. 90, pp. 119–133, 2019.
- [57] C. Yu, J. Wang, C. Peng, C. Gao, G. Yu, and N. Sang, "Learning a discriminative feature network for semantic segmentation," in *Proceedings of the IEEE Conference on Computer Vision and Pattern Recognition*, pp. 1857–1866, 2018.
- [58] H. Zhao, Y. Zhang, S. Liu, J. Shi, C. Change Loy, D. Lin, and J. Jia, "Psanet: Point-wise spatial attention network for scene parsing," in *Proceedings of the European Conference on Computer Vision (ECCV)*, pp. 267–283, 2018.
- [59] Y. Yuan, X. Chen, and J. Wang, "Object-contextual representations for semantic segmentation," *arXiv preprint arXiv:1909.11065*, 2019.